Comparative characterization of the surface state of Ti-6Al-4V substrates in different pre-bonding conditions

M. Pizzorni [a,c,*], E. Lertora [a], C. Mandolfino [a], S. Vicini [b], M. Salerno [c], M. Prato [c]

[a] Department of Mechanical Engineering, Polytechnic School, University of Genoa, Via All'Opera Pia 15, Genoa 16145, Italy
[b] Department of Industrial Chemistry, University of Genoa, Via Dodecaneso 31, Genoa 16146, Italy
[c] Materials Characterization Facility, Istituto Italiano di Tecnologia, Via Morego 30, Genova 16163, Italy

ARTICLE INFO

ABSTRACT

This paper deals with the interfacial adhesion properties of Ti-6Al-4V alloy substrates, prepared by using different treatment protocols selected on the basis of their different effectiveness, and bonded using a structural, high-strength epoxy adhesive. The alternative pre-bonding treatments were sodium hydroxide anodization and low-pressure-plasma treatment, the effects of which were compared to that of a base preparation via solvent degreasing of the substrates' surface. The treated surfaces were joined according to standard protocols, and then tested for shear strength. The mechanical results were then correlated to surface characteristics of the substrates such as oxidation state and wettability. Parallel scanning Kelvin-probe measurements allowed us to focus our attention on the possible role of the electrical properties of the substrates. We observed that each treatment entails different behavior of the electrical potential of the surface, which correlates with the mechanical strength of the joints. The results suggest that an evaluation of the surface potential of titanium-alloy substrates might be a promising, indicative supplementary parameter for the evaluation of their pre-bonding surface conditions, allowing correlations with presence/absence of an oxide layer at the resin-substrate interface.

Introduction

Adhesive bonding is one of the most common processes for assembly operations of titanium-alloy products, which are difficult to join by means of traditional welding technologies, and for which mechanical fastening is often avoided (Wegman and Van Twisk, 2013). Indeed, thanks to the ongoing developments of high-performing resins, along with rigid process protocols, many manufacturing industries are exploiting this joining method more and more in applications requiring high strength, toughness, reliability and durability for assemblies (Ebnesajjad, 2009). The use of adhesive bonding may allow one to obtain final structures having optimal mechanical characteristics without deforming the base material, minimizing stress concentrations, and also preserving lightness (Davis and Bond, 1999).

Nevertheless, to achieve these properties, strict control of the conditions at the adhesive-material interface has to be guaranteed during the process. The desired joint performance can indeed be achieved only through specific pre-bonding treatments on the substrates, able to create the chemical, mechanical and/or electrical conditions needed to guarantee the formation of stable resin-material bonds.

In this work, different surface treatments were performed for the preparation of adhesive joints in Ti-6Al-4V alloy in order to obtain surface conditions that were effectual or critical for adhesive bonding. In particular, low-pressure plasma (LPP) and sodium-hydroxide anodization (SHA) treatments were compared on the basis of the wide knowledge of their different effectiveness on titanium substrates (Molitor et al., 2001; Akram et al., 2010; Ebnesajjad, 2009; Lim et al., 2001).

Titanium alloys naturally form a passivation oxide film on their surface at equilibrium (Zhang et al., 2020). Such behavior entails a weak boundary condition for adhesive bonding, because the oxide becomes a fragile interlayer between the adhesive and metal bulk. As demonstrated by Akram et al. (2010), this may be detrimental for the performance of adhesive joints and, often, does not allow the attainment of the targeted requirements for the application. In view of such considerations, evaluations of the chemical state, of the wetting properties and of the roughness of substrates have to be compared with the mechanical testing results. In particular, contact-angle measurement is a common practice to qualitatively establish the capability of a substrate of being wet by an adhesive (N'guessan et al., 2013). In principle, the higher the surface free energy, the better a liquid drop spreads on the surface. Nevertheless, the physical behavior of the droplet is remarkably affected by the surface condition, namely, roughness, heterogeneities, and oxidation state. Therefore, it is not uncommon to obtain false-positive results.

We discussed this aspect in a preliminary work (Pizzorni et al., 2018), where we obtained low-performance joints in Ti-6Al-4V alloy, despite the surfaces being hydrophilic, owing to oxidation brought about by LPP treatment. In contrast, Gómez-Méndez et al. (2018) observed highly-hydrophobic behavior of Ti-6Al-4V surfaces after different anodization procedures, attributing this behavior to the air trapped inside the pores of the anodic layer. These inconsistent results are thus exemplificative of the limits of wettability as an evaluation method for adhesive bonding. On the other hand, they highlight the need of considering the interface with a more empirical approach.

It is worth noting that, even in this work, the results obtained from measurements of contact angle performed to estimate the surfaces wetting properties led to similar conclusions. Further investigations were hence necessary about the chemical and physical phenomena occurring on the surface due to treatments. In particular, an X-ray photoelectron spectroscopy (XPS) analysis was also carried out to quantify the amount of oxidized species of Ti. The results were then compared to those obtained from an electrical potential mapping of the surfaces, performed by using scanning Kelvin probe microscopy (SKPM). Interestingly, the different chemistry of the differently-treated surfaces determines changes of the sample surface potential, hence suggesting SKPM as a possible complementary method to evaluate the interfacial conditions of Ti-6Al-4V alloy in adhesive bonding.

Given the novelty of SKPM in the adhesive-bonding field, a brief description of this technique will be provided as Annex of the paper. This background information can help in the interpretation of the results.

Experimental details

Materials

In this investigation, an alpha-beta stabilized titanium alloy, Ti-6Al-4V, also known as Grade 5 (ASTM B 265), was used as the substrate material. The joints were manufactured by using a high-temperature-resistant, structural epoxy adhesive, Hysol EA-9394 (Loctite, Düsseldorf, Germany). The adhesive paste was prepared by mixing 100 parts of epoxy resin and 17 parts of curing agent, as indicated by the product data sheet. Curing consisted of a 24 h stay at room temperature and subsequent post-curing in an oven at 66°C for one hour.

Surface preparation and treatments

Before each treatment, all samples were wiped with a cotton cloth soaked with acetone to remove any traces of dust or organic contaminants. The pre-bonding preparation of the substrates involved different processes, and the following sets of samples were produced:

CTRL: this set of control samples consisted of degreased-only substrates/joints, and was used as a reference, representing the base pre-bonding condition of the surfaces before further treatment;

PL: these substrates underwent LPP treatment, performed using a Tucano (Gambetti, Milan, Italy) plasma reactor of 200 W maximum nominal power (acting on a sample-support plate of dimensions 110×300 mm), supplied by a radio-frequency generator operating at 13.56 MHz. All substrates were inserted into the chamber and this was evacuated down to a pressure of 0.4 mbar. Then, the process gas was introduced into the chamber, causing a slight over-pressure to 0.5 mbar. In this condition, the device was switched on to ignite the glow discharge. The aforesaid pressure level was kept constant over the entire duration of treatment. The LPP treatment was performed using atmospheric air, and process power and exposure time were set at 125 W and 160 s, respectively, based on preliminary screening among different process-parameter combinations.

SHA: the surfaces belonging to this set of samples were treated with sodium-hydroxide anodization. This treatment consisted of electrochemical positive polarization in a 5 M sodium hydroxide (NaOH) (used as the electrolyte) after a preliminary hydrofluoric acid/nitric acid

Table 1
Polar, disperse and total surface tension of test liquids.

Liquid	γ_L^p (mN/m)	γ_L^d (mN/m)	γ_L (mN/m)
H_2O	51	21.8	72.8
CH_2I_2	0	50.8	50.8

pickling – performed in 15% by volume of 70% HNO_3 and 3% by volume of 50% HF – and further rinsing in running water (Ingram and Ramani, 1997);

Surface characterization

Chemical state evaluation and contact angle measurements

An Axis Ultra[DLD] (Kratos, Manchester, UK) spectrometer was used to perform XPS analyses. The instrument is equipped with a monochromatic Al Kα source (photon energy = 1486.6 eV) operating at 15 kV and 20 mA. All analyses were carried out on a 300×700 μm^2 area, keeping the analysis chamber in UHV conditions ($p < 6 \times 10^{-9}$ mbar) during data acquisition. The high-resolution scans were performed at a pass energy of 20 eV and steps of 0.1 eV on the energy range typical for Ti 2p peak. All spectra were charge calibrated to the main line of the C 1 s spectrum (C-C bonds), setting its binding energy value at 284.8 eV. Spectra analyses (peak deconvolution and data fitting) were performed with the CasaXPS software (version 2.3.18), setting Shirley-type background.

Wettability of the surfaces was evaluated through measurements of contact angle (CA) of two different test liquids, namely, deionized (DI) water and diiodomethane (CH_2I_2), chosen on the basis of their opposite polar behavior. The polar (γ_L^p) and disperse (γ_L^d) components of surface tension of these liquids are reported in Table 1.

The assessment was performed with a Theta Lite (Biolin Scientific, Gothenburg, Sweden) optical tensiometer, working in sessile-drop mode. Since the effect of gravity is gradually weakened as the drop volume decreases (Sakai and Fujii, 1999), in this investigation, the latter was kept constant and equal to 3 μL for DI water and 2 μL for CH_2I_2, differently chosen to partly compensate for their different density. The measurements were performed depositing six droplets per probe liquid on the substrate. For each droplet, the CA was determined as the mean between the two values acquired at the right and left side of the drop profile. The relative images were captured and then digitized using the instrument software, One Attension.

Roughness and electrical potential measurements by SKPM

Both roughness and electrical potential assessment were performed on the surfaces of the substrates with microscale local spatial resolution by means of SKPM technique, using an atomic force microscope MFP-3D (Asylum Research – Oxford Instruments, Santa Barbara, CA, USA).

The probes used were MESP (Bruker, Billerica, MA, USA), with cantilevers of nominal resonance frequency of 75 kHz and tips of nominal apex radius of 35 nm, coated with a 25 nm layer of CoCr alloy. The measurements were performed in double-pass mode, acquiring the topographic profile during the first pass (from which the RMS roughness Sq was extracted), and then flying over the same profile at a given elevation distance of 100 nm during the second pass, to measure the electrical potential on the sample surface, U_s. During measurement, the samples edges were painted with silver paste, and then connected to ground by means of adhesive copper tape. For each sample, the mean value of U_s was acquired as an average of three 40×40 μm^2 scans on randomly selected portions of surface, spaced a few millimeters apart.

Data processing and post-processing of images were performed by using the Asylum Research AFM program version 16, developed under software platform Igor Pro 6.22 (WaveMetrics, Lake Oswego, OR, USA).
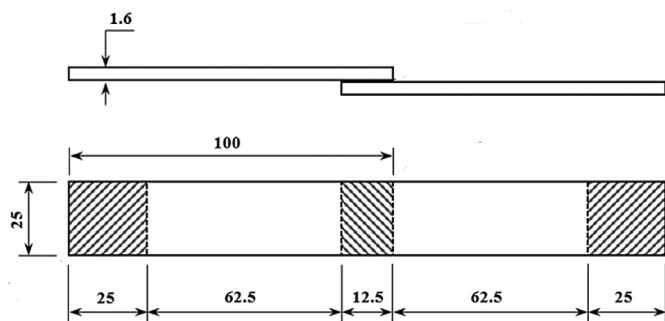
Fig. 1. Single-lap joint geometry (values in mm), according to ASTM D 1002.

Table 2

Chemical composition of the sample surfaces differently treated, expressed in atomic percentage.

Surface treatment	O 1 s	C 1 s	Ti 2 p	Al 2 p	V 2 p	Others
CTRL	26.4	57.4	5.1	1.4	0.3	9.4
PL	40.9	38.5	8.9	2.9	0.4	8.4
SHA	40.8	32.7	16.6	2.9	0.7	6.3

Adhesive-joint fabrication and mechanical testing

For each set of the aforementioned treatment conditions, five single-lap joints ($N = 5$) were made in accordance with the ASTM D 1002 standard (Fig. 1) (ASTM D 1002-05, 2005). The Loctite Hysol EA-9394 adhesive was applied to the bond area of both substrates. The two laminates were placed together, positioned with a 12.5 mm overlap. A controlled thickness of adhesive (0.05 mm) was obtained using a sheet of non-stick paper of calibrated thickness. Any excess adhesive at the interface was expelled by pressing the joint and then removed. The resulting adhesive joint was finally cured according to the procedure previously described.

The mechanical characteristics of adhesively-bonded joints were evaluated in terms of tensile shear strength (TSS). The joints were tested to failure at a crosshead displacement rate of 1.3 mm/min using an 8802 Universal Testing machine (Instron, Norwood, MA, USA) equipped with a 50 kN load cell. A grip area of 25×25 mm was ensured. Tabs having the same thickness as the titanium laminates (1.6 mm) were positioned at the grip areas, to align the bond area along the centerline between the grip faces.

Results

XPS assessment was performed on the differently treated substrates (the chemical compositions of which are reported in Table 2), focusing on the surface oxidation state of Ti; the results are presented in Fig. 2. This displays the high-resolution spectra of the characteristic doublet structure of the Ti 2p peak, related to the CTRL, PL and SHA surfaces, respectively. The deconvolution of the Ti 2p peak allowed the identification of the chemical species involved in the oxidation state of the specimen surfaces: two peaks at about 459 eV and 464 eV corresponding to titanium (IV)oxide (Ti^{4+}), two peaks at 457 eV and 462.5 eV representative of titanium (III)oxide (Ti^{3+}), and a doublet at about 453.5 and 460 eV corresponding to the metallic component of titanium (Ti^0). A further doublet corresponding to titanium (II)oxide (Ti^{2+}) was detected on the SHA sample, with peaks at 455.5 eV and 470 eV (Biesinger et al., 2010). By quantifying such species in terms of atomic percentage (at.%), it was observed that the LPP treatment entailed a considerable increase of the oxidized species. In contrast, the amount of Ti^0 on the SHA surface resulted 18.0 at.%, against 4.8 at.% and 3.6 at.% of the CTRL and PL surfaces, respectively.
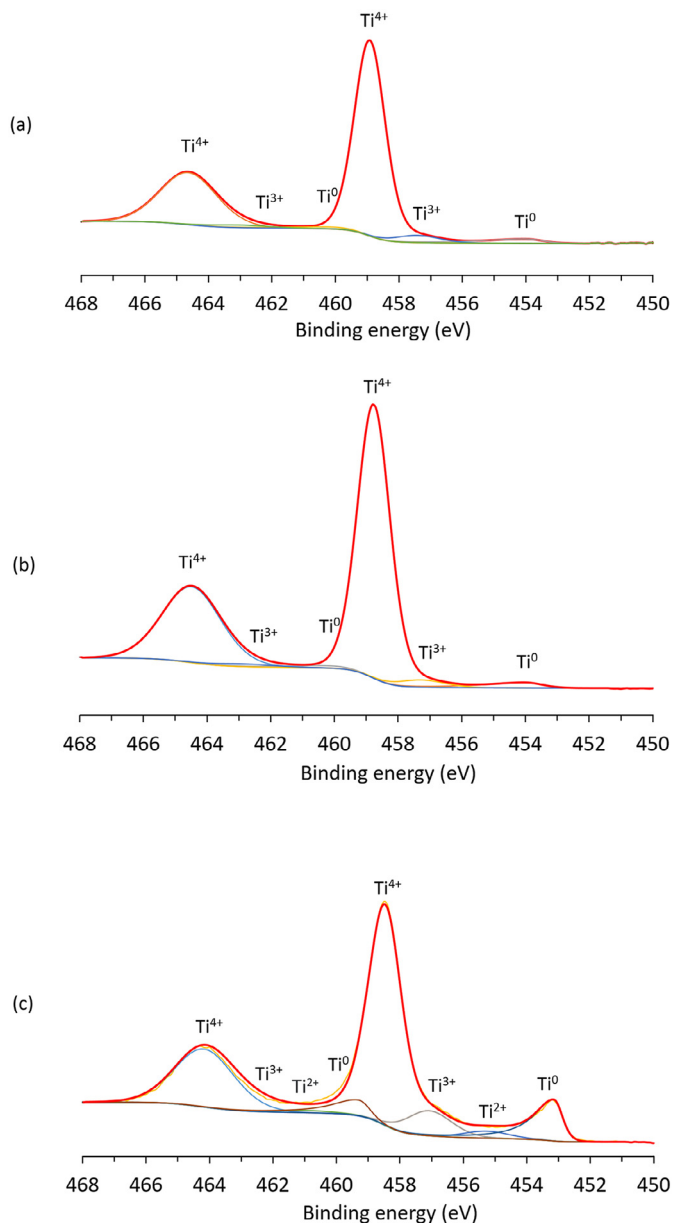

Fig. 2. High-resolution XPS spectra of the Ti 2p peak of (a) the reference CTRL-sample, (b) PL-sample and (c) SHA-sample surfaces.

In parallel, the wetting properties of the sample surfaces were evaluated on the basis of the measurements of CA, the results of which are reported in Table 3. The relative insets show typical pictures of the sessile drops of the two test liquids, acquired for the measurement. In particular, after deposition on the reference surface (CTRL), the droplets of DI water and CH_2I_2 presented values of apparent CA that were nearly identical on average ($63.4° \pm 1.2°$ and $62.1° \pm 1.0°$, respectively). Higher hydrophilicity emerged on the plasma-treated surfaces (PL), which exhibited water-CA of $23.0° \pm 2.1°$, whereas that of CH_2I_2 stood at $34.6° \pm 0.8°$. A completely opposite condition was observed on the SHA surface, which exhibited quasi-hydrophobic properties, with CA values of $93.9° \pm 2.6°$ and $59.2° \pm 1.6°$ for DI water and CH_2I_2, respectively.

As a surface characterization technique complementary to wettability measurements, in this work, the SKPM analysis was carried out. For the related results, the reader is invited to refer again to Table 3. It should be mentioned that, for the values of electrical surface potential

Table 3
Summary of the main results of the XPS, CA, AFM and SKPM measurements.

Sample	XPS	Wettability		Roughness	Electrical potential
	Ti^0 / Ti^{4+} (%)	θ_{H_2O} (deg)	$\theta_{CH_2I_2}$ (deg)	Sq (μm)	U_S (mV)
CTRL	5.3	63.4 ± 1.2	62.1 ± 1.0	0.69 ± 0.06	$+5 \pm 38$
PL	3.4	23.0 ± 2.1	34.6 ± 0.8	0.90 ± 0.13	-358 ± 49
SHA	25.7	93.9 ± 2.6	59.2 ± 1.6	0.28 ± 0.04	$+408 \pm 33$

U_S, a relevant dispersion around the means was observed in SKPM, due to both local heterogeneities of the surface (corresponding to the inner contrast of the maps shown in Fig. 3) and variations between different portions of the same specimen, which were all sampled and averaged.

Simultaneous roughness measurements highlighted that both the CTRL and PL samples exhibited Sq values (0.67 ± 0.06 μm and 0.90 ± 0.13 μm, respectively) that were higher than those measured on the SHA-treated surface (0.28 ± 0.04 μm). This observation of a surface smoothing, occurring on the latter sample during anodization, can be interpreted as a result of electro-polishing occurring during the respective treatment.

From the parallel analysis of electrical potential, the CTRL substrate exhibited mean value of U_s, positive on average but ranging around neutrality considering the standard deviation ($+5 \pm 38$ mV). In turn, the PL sample showed U_s equal to -358 ± 49 mV, namely, significantly different from zero in modulus and negative in sign. Conversely, the SHA surface was characterized by high positive values of the electrical potential ($+408 \pm 33$ mV).

A further set of Ti-6Al-4V substrates (named SHA-AGED) was chemically treated in the same conditions as the former. After treatment, the laminates were then exposed to ambient conditions (temperature of 25 °C, relative humidity of 50%) for 15 days, to make the treatment effect age.

By performing sessile-drop analysis on the chemically-treated surface after aging, compared to the fresh SHA surface, a reduction of the water-CA values ($52.6° \pm 13.6°$), along with an increase of those obtained with CH_2I_2 ($67.9° \pm 8.13°$), were observed. On the basis of the previous considerations, this behavior is reasonably related to the increased oxidation state of the surface during aging. Indeed, the XPS analyses carried out on the SHA-AGED surface highlighted a decrease of the metallic component to 7.2 at.%, and a corresponding increase of the amount of oxidized species.

Finally, SKPM was carried out on the SHA-AGED substrate, resulting in a surface potential of $+133 \pm 8$ mV, namely, again positive in sign but about 67% lower than the value acquired immediately after treatment.

The results of the TSS testing, grouped according to the different pre-bonding preparations, are presented in Fig. 4. The height of the bars represents the mean value of TSS (expressed in MPa), whereas the error bars at the bar tops represent the standard deviation around each respective mean.

The effectiveness of the electrochemical treatment (SHA) in increasing the adhesion properties of the titanium substrate with respect to the control (CTRL) is evident. The mean TSS of the former was almost 3.5 times that of the CTRL sample, reaching up to 32 ± 2 MPa. In turn, when LPP treatments were performed, no deviation from the maximum load achieved by the reference samples was observed, despite the stiffness of the PL sample being slightly reduced. These results were confirmed by the different fracture mode obtained after complete failure, which was mixed in type (i.e., cohesive within the adhesive layer and partly de-adhesive) for the SHA joints (Fig. 4c), whereas it was completely de-adhesive in type for both the CTRL and the PL joints (Fig. 4a,b).

Five additional SHA-AGED joints were also manufactured, following the same procedure described previously. The specimens were then tested for shear, resulting in a reduction of 41.6% in TSS with respect to the newly-treated SHA sample.

Discussion

TSS testing confirmed a remarkable difference between the mechanical behavior of the PL and SHA joints. In fact, the poor adhesive properties presented by the LPP-treated joints were not unexpected, since inherently linked to the weak adhesion conditions at the interface brought about by plasma on titanium already observed in the literature (Akram et al., 2010). Indeed, as also detected via XPS, the air-plasma treatment of Ti-6Al-4V generated an oxide layer on the surface. In accordance with the weak-boundary-layer theory by Bikerman (1967), the presence of this TiO_2 film caused the rapid, brittle detachment of the two joined laminates as soon as the film failed, entailing joint failure that was completely de-adhesive in type. In turn, the SHA joints exhibited TSS that was more than threefold that of the PL joints. The effectiveness of SHA treatment in creating stable interface conditions with adhesive was made clear by the mixed cohesive failure of the joints, to which the increase of the metallic component Ti^0 (and simultaneous reduction in the amount of TiO_2) also contributed. A confirmation of this has been found when testing the SHA-AGED samples, whose reduction in performance was matched by a new decrease in the Ti° component at the interface.

Whereas a correspondence between mechanical characteristics (performance and failure mode) and surface chemical state has been reasonably determined, the same does not hold true for wettability. As previously remarked, evaluation of the wettability is one of the most common practices to macroscopically estimate the adhesive properties of a substrate to be adhesively-bonded. Conventionally, it is however defined as a "necessary but not sufficient condition" since, to validate its reliability, such an evaluation should be supported by a number of further experimental assessments able to confirm or justify the behavior of the droplet. Despite it provides an indication of the capability of a surface of being coated, this assessment is indeed strictly dependent on the variability of the surface finishing conditions: surface oxidation state (Lim et al., 2001), but also roughness extent and profile, or heterogeneities due to air trapped in micro-pores (N'guessan et al., 2013). Indeed, as also observed by Terriza et al. (2011), static CA measurements
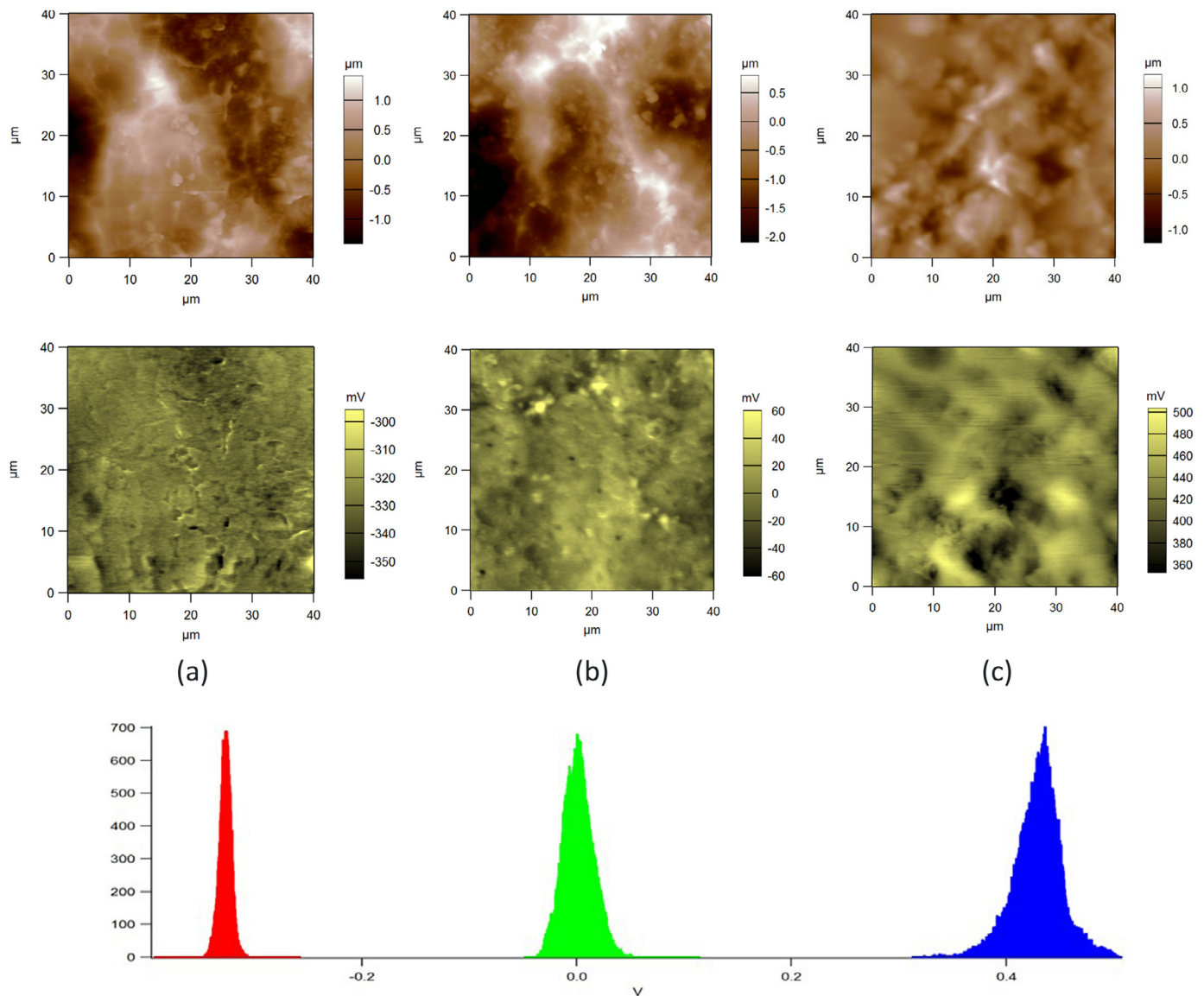
Fig. 3. Relative surface height (top maps) and distribution of electrical potential U_S (bottom maps) on three representative cases of sample areas of (a) PL, (b) CTRL and (c) SHA sample. A histogram plot reporting the values of U_S measured on each surface is also provided.

are severely affected by surface roughness and other morphological parameters that are used to deduce the equivalent value of CA from those measured. The higher roughness values, the more critical the determination of the scale of measurement, and, hence, significant errors may occur also in the calculation of equivalent CAs.

In any case, the values of CA measured on both the CTRL and PL samples were in agreement with the results of a former work by Pizzorni et al. (2018) and found further confirmation in some studies by Oshida et al. (1992), (1993). Notably, the intense surface activation, along with the increased surface oxidation, were the reasons for the hydrophilic behavior exhibited by the PL sample. Conversely, the surface of the anodized sample (SHA) appeared to be quasi-hydrophobic, as also found by Gómez-Méndez et al. (2018). In principle, wettability should provide indications about the capability of the adhesive to penetrate into any substrate asperity, increasing the actual contact area and, consequently, the substrate-to-resin interactions. Nevertheless, given the excellent mechanical performance of the corresponding SHA joints, the present results are clearly in disagreement with such a principle, and wettability of the surface does not appear to be "necessary" for good adhesion and consequent joint strength.

Due to inconsistency between the CA measurements and mechanical results, an alternative approach to surface characterization was adopted, via SKPM analysis. This technique may describe the electrical conditions generated on the substrate surfaces after treatments. Based on the experimental findings, a relationship seems to exist between surface potential U_S and TiO_2 oxide layer. In particular, the amount of titanium dioxide on the PL-sample surface appeared to be a concomitant cause for negative values of U_S. In contrast, the SHA-sample surface presents lower amount of oxidized species, but higher exposed Ti^0, hence resulting in U_S positive in sign.

For critical interpretation of the results, it should be noted that the value of U_S depends on a combination of co-factors, including the electron work function (EWF) of both the sample and probe tip metals, and the presence of possible electrostatic charge, which in turn depends on former contact history (e.g., possible triboelectric effect) and on environmental conditions (in particular, ambient relative humidity) (Salerno and Dante, 2018). As a secondary effect, the EWF of the sample can also depend on surface contaminants (Abdellatif et al., 2016), as well as on the material surface roughness (Xue et al., 2012). Given this variety of side-effects, the U_S values obtained with different probe tips
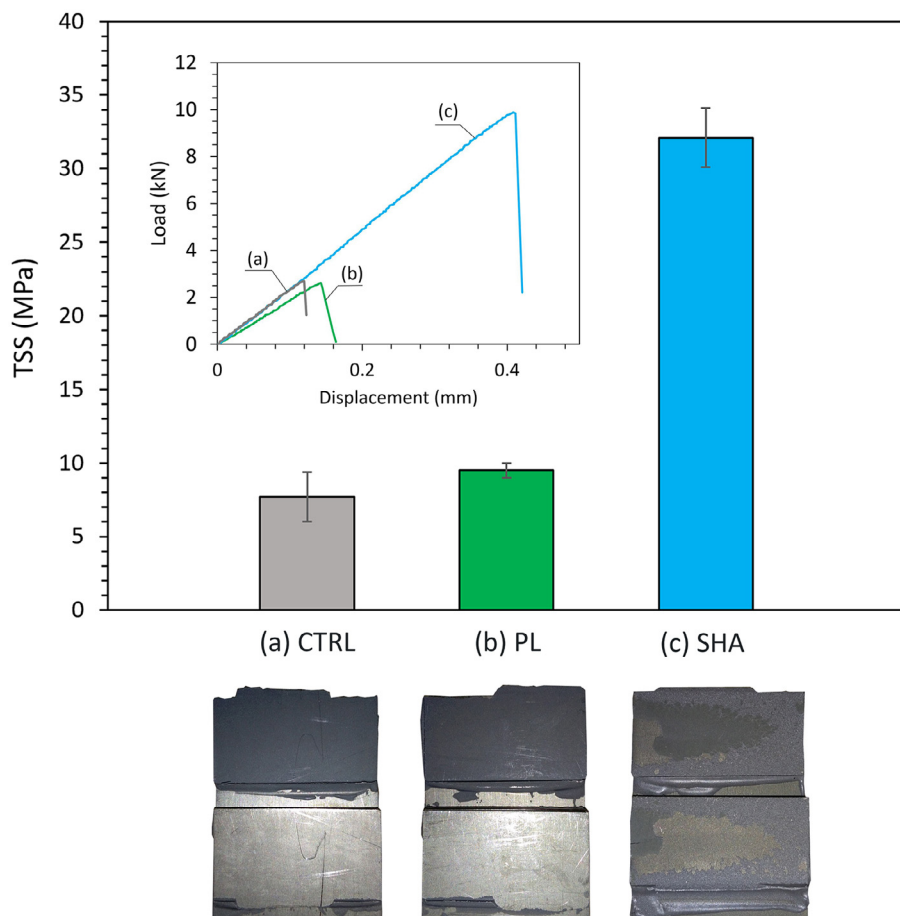
Fig. 4. Summary of the TSS results of adhesively-bonded joints obtained after different treatments of the substrates. In the inset, representative load-displacement curves are displayed of (a) CTRL, (b) PL and (c) SHA joints. The typical fracture surfaces obtained after mechanical testing of the relative joints are also shown.

(coated with a different metal and different thickness, and thus resulting in different tip EWF) could be all shifted with respect to the presently observed zero. Therefore, more than the absolute U_S values, the relative differences between different samples should be considered, as the more robust hint of different electrical states of the substrate surfaces. Within the mentioned limitations, if the different observed U_S is still ascribed mainly to differences in sample surface EWF_S, i.e., to the material surface chemistry effects, one can explain why the CTRL and PL samples – despite having Ti 2p showing almost similar degree of oxidation – presented different U_S, in correlation with the different chemical composition of the surfaces (Table 2). However, when aging of the SHA surface was carried out, the most significant effect observed was the increased oxidation. Therefore, it is reasonable to believe that the re-oxidation occurred during aging (SHA-AGED samples) remarkably contributed to the decrease of the U_S intensity with respect to the newly-treated SHA sample.

Conclusion

In this work, the adhesion properties of Ti-6Al-4V substrates in different treatment conditions were evaluated. In particular, the comparison involved samples the surfaces of which have been treated for adhesive bonding by means of LPP or SHA, taking solvent degreasing as a reference preparation. The treatment effects were critically analyzed in terms of mechanical performance of adhesive joints, surface oxidation and wettability. The experimental findings were then correlated to measurements of surface electrical-potential performed via SKPM technique. Our comparative analysis allowed us to obtain useful information about the response of these adhesive systems, making it possible to identify the electrical potential assessment of the substrate surfaces as an alternative method to evaluate the adhesion interfacial properties of Ti sub-

strates. Notably, the results suggested that, using Ti-6Al-4V substrates, a relationship between higher (positive) values of the electrical surface potential U_S and the SHA treatment exists, whereas LPP leads to lower (negative) values of U_S. Sign and intensity of U_S seem to be successfully related to the mechanical performance of adhesively-bonded joints, the former representing a parameter that may be associated with the oxidation state of the surface. Indeed, a rest-time after treatment determines a decrease of the mechanical performance of the joints, which is related to the surface re-oxidation.

Declaration of Competing Interest

The authors declare that they have no known competing financial interests or personal relationships that could have appeared to influence the work reported in this paper.

Annex. Scanning Kelvin probe microscopy

SKPM is a scanning probe microscopy technique (particularly, an advanced version of electric force microscopy) that allows both a topographic mapping and a semi-quantitative evaluation of the sample surface contrast in electrical potential, thanks to a double-scan acquisition mode. A schematic of the configuration adopted for the SKPM measurements is shown in Fig. A1. In the implementation of the currently used setup, the sample is ideally grounded, whereas the tip is set to a positive voltage, which generates an electric force on the probe. In particular, the tip voltage has one DC and one AC component, such that the total voltage difference between tip and sample at any time is as follows:

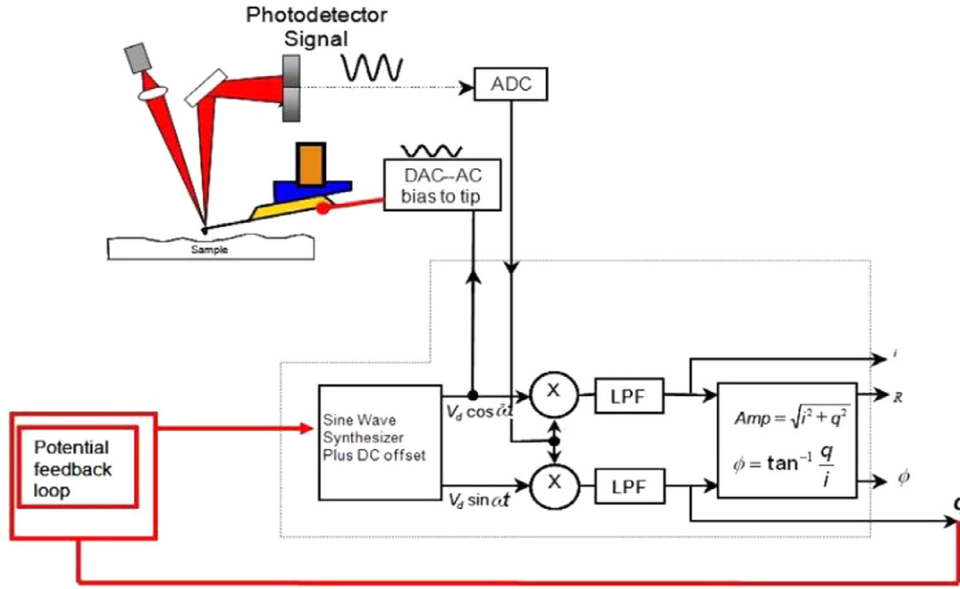$$U = U_{DC} - U_s + U_{AC} \ \sin{(\omega t)} \tag{A1}$$

Fig. A1. Operating scheme of the SKPM device used (reproduced with permission from the manual of the Asylum Research MFP-3D (Asylum Research, 2013)).

where U_{DC} is the DC component of tip bias, U_{AC} and ω are the amplitude and frequency of the AC component of the tip bias, and U_s is the electrical surface potential emerging on the sample surface due to different additive effects: electrostatic charging, difference in EWF between tip and sample metals, and possible extra voltage applied to the sample. In ideal conditions, the other two contributions are null, so that it is $U_S = (\text{EWF}_t - \text{EWF}_S)/e$ (with obvious meaning of the subscripts, and e being the electron charge) what is called contact potential difference (arising only on tip-sample contact, see (Salerno and Dante, 2018)). Actually, whereas EWF_t is constant over the scanned area, EWF_S is not, such that $U_s = U_s(x, y)$, the spatial maps appearing like the images in Fig. 3. The U_S is detected via the cantilever force sensor assembled together with the tip, according to the point that the tip and sample metals work like the plates of a capacitor, according to which, the force between them is:

$$F = \left[(\partial C/\partial z)\, U^2\right]/2 \tag{A2}$$

A region of space Δz above the sample is actually explored by the probe, as the driving AC frequency corresponds to the mechanical resonance frequency of the cantilever, which makes it oscillate inside the electrical field, giving rise to force F. By substituting Eq. (A1) for the term U^2 in Eq. (A2), one obtains:

$$U^2 = \left(U_{DC} - U_s\right)^2 + 2\left(U_{DC} - U\right)U_{AC}\sin(\omega t) + U_{AC}^2 \sin^2(\omega t) \tag{A3}$$

and, since $\sin^2(\theta) = \frac{1}{2}[1 - \cos(2\theta)]$, this becomes:

$$U^2 = \left(U_{DC} - U_s\right)^2 + 2\left(U_{DC} - U_s\right)U_{AC}\sin(\omega t) + \frac{1}{2}U_{AC}^2[1 - \cos(2\omega t)] \tag{A4}$$

Accordingly, in Eq. (A2), one has $= F_1 + F_2 + F_3$, where:

$$F_1 = \frac{1}{2}\frac{\partial C}{\partial z}\left[\left(U_{DC} - U_s\right)^2 + \frac{1}{2}U_{AC}^2\right] \tag{A5}$$

$$F_2 = \frac{\partial C}{\partial z}\left[\left(U_{DC} - U_s\right)U_{AC}\sin(\omega t)\right] \tag{A6}$$

$$F_3 = -\frac{1}{4}\frac{\partial C}{\partial z}U_{AC}^2\cos(2\omega t) \tag{A7}$$

Notably, both F_1 (which is DC) and F_3 (which occurs at twice as much the required frequency) are not enhanced by the cantilever resonance. Therefore, most force is given by F_2, which is proportional to

the difference of DC component of tip bias and sample potential U_S. It follows that F assumes its minimum value if $U_{DC} - U_s = 0$.

The force signal is thus fed into a proportional-integral feedback loop circuit, which makes it such that, at each time instant and point on the sample, U_S can be obtained as the DC tip bias component necessary for proper zeroing the error. More details on SKPM operation may be found in Lanza (2017).

References

Abdellatif, MH, Ghosh, S, Liakos, I, Scarpellini, A, Marras, S, Diaspro, A, et al., 2016. Effect of nanoscale size and medium on metal work function in oleylamine-capped gold nanocrystals. J. Phys. Chem. Solids 89, 7–14. doi:10.1016/j.jpcs.2015.09.012.

Akram, M, Bhowmik, S, Jansen, KMB, Ernst, LJ., 2010. Surface modification of titanium by atmospheric pressure plasma treatment for adhesive bonding and its application to aviation and space. In: Proceedings of the SAMPE Europe 31st International Technical Conference Forum.

ASTM D 1002-05. Standard Test Method for Apparent Shear Strength of Single-Lap-Joint Adhesively Bonded Metal Specimens by Tension Loading (Metal-to-Metal). Standards 2005:1–5. doi:10.1520/D1002-10.on.

Asylum Research, 2013. SPM Applications Guide. Asylum Research, p. 168.

Biesinger, MC, Lau, LWM, Gerson, AR, Smart, RSC., 2010. Resolving surface chemical states in XPS analysis of first row transition metals, oxides and hydroxides: Sc, Ti, V, Cu and Zn. Appl. Surf. Sci. 257, 887–898. doi:10.1016/j.apsusc.2010.07.086.

Bikerman, JJ., 1967. Causes of poor adhesion: weak boundary layers. Ind. Eng. Chem. 59, 40–44. doi:10.1021/ie51403a010.

Davis, M, Bond, D., 1999. Principles and practices of adhesive bonded structural joints and repairs. Int. J. Adhes. Adhes. 19, 91–105. doi:10.1016/S0143-7496(98)00026-8.

Ebnesajjad, S., 2009. Material surface preparation techniques. In: Adhesives Technology Handbook, pp. 37–46. doi:10.1016/b978-0-8155-1533-3.50006-2.

Ebnesajjad, S., 2009. Adhesive applications and bonding processes. In: Adhesives Technology Handbook, pp. 183–208. doi:10.1016/b978-0-8155-1533-3.50011-6.

Gómez-Méndez, M, Durán-Pabón, C, Naranjo, DI, Arenas, MA, Garciá-Vergara, SJ., 2018. Anodizing of Ti6Al4V alloy for aeronautical applications. J. Phys. Conf. Ser. 1119. doi:10.1088/1742-6596/1119/1/012028.

Ingram, C, Ramani, K., 1997. The effect of sodium hydroxide anodization on the durability of poly(etherketonetherketoneke-tone) adhesive bonding of titanium. Int. J. Adhes. Adhes. 17, 39–45. doi:10.1016/S0143-7496(96)00027-9.

Lanza, M., 2017. Conductive Atomic Force Microscopy: Applications in Nanomaterials. John Wiley & Sons.

Lim, YJ, Oshida, Y, Andres, CJ, Barco, MT., 2001. Surface characterizations of variously treated titanium materials. Int. J. Oral Maxillofac. Implant. 16, 333–342.

Molitor, P, Barron, V, Young, T., 2001. Surface treatment of titanium for adhesive bonding to polymer composites: a review. Int. J. Adhes. Adhes. 21, 129–136. doi:10.1016/S0143-7496(00)00044-0.

N'guessan, HE, White, R, Leh, A, Baksi, A, Tadmor, R, 2013. Fundamental understanding of drops wettability behavior theoretically and experimentally. In: Advances in Contact Angle, Wettability and Adhesion. John Wiley & Sons, Ltd, pp. 87–96. doi:10.1002/9781118795620.ch5.

Oshida, Y, Sachdeva, R, Miyazaki, S, Daly, J., 1993. Effects of shot-peening on surface contact angles of biomaterials. J. Mater. Sci. Mater. Med. 4, 443–447. doi:10.1007/BF00120123.

Oshida, Y, Sachdeva, R, Miyazaki, S., 1992. Changes in contact angles as a function of time on some pre-oxidized biomaterials. J. Mater. Sci. Mater. Med. 3, 306–312. doi:10.1007/BF00705298.

Pizzorni, M, Gambaro, C, Lertora, E, Mandolfino, C., 2018. Effect of process gases in vacuum plasma treatment on adhesion properties of titanium alloy substrates. Int. J. Adhes. Adhes. 86, 113–122. doi:10.1016/j.ijadhadh.2018.07.007.

Sakai, H, Fujii, T., 1999. The dependence of the apparent contact angles on gravity. J. Colloid Interface Sci. 210, 152–156. doi:10.1006/jcis.1998.5940.

Salerno, M, Dante, S., 2018. Scanning kelvin probe microscopy: challenges and perspectives towards increased application on biomaterials and biological samples. Mater 11. doi:10.3390/ma11060951, (Basel, Switzerland).

Terriza, A, Alvarez, R, Yubero, F, Borras, A, González-Elipe, AR., 2011. Comments on "an essay on contact angle measurements": determination of surface roughness and modeling of the wetting behavior. Plasma Process. Polym. 8, 998–1002. doi:10.1002/ppap.201100081.

Wegman, RF, Van Twisk, J., 2013. Surface Preparation Techniques for Adhesive Bonding, 2nd Ed. Elsevier doi:10.1016/B978-1-4557-3126-8.00003-8.

Xue, M, Wu, H, Ou, J, Wang, F, Li, X, Li, W, et al., 2012. On the correlation between surface morphology and electron work function of indium tin oxide. J. Appl. Phys. 111. doi:10.1063/1.4730388.

Zhang, LC, Chen, LY, Wang, L, 2020. Surface modification of titanium and titanium alloys: technologies, developments, and future interests. Adv. Eng. Mater. 22. doi:10.1002/adem.201901258.